

# Conductive Hydrogels with Topographical Geometry and Mechanical Robustness for Enhanced Peripheral Nerve Regeneration

Yinghui Feng,<sup>2</sup> Liangjie Shan,<sup>2</sup> Yafei Wang, Xingmei Chen, Chang Wang, and Ji Liu\*



Cite This: <https://doi.org/10.1021/acsnano.5c00845>



Read Online

ACCESS |

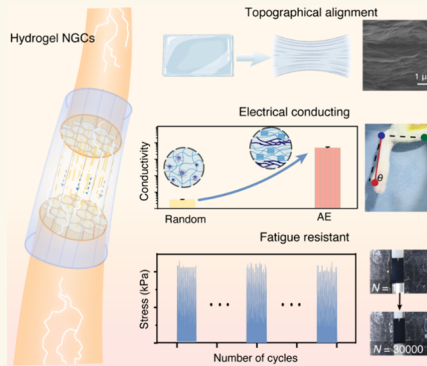
Metrics & More

Article Recommendations

Supporting Information

**ABSTRACT:** Nerve guidance conduits (NGCs) emerge as a promising solution for nerve regeneration; however, conventional NGCs fail to fulfill the requirements for peripheral nerve regeneration, which are subjected to periodical yet vigorous stretching, bending, and compression. Here, we developed a fatigue-resistant conductive hydrogel-based NGC by integrating topographical geometry, enhanced electroactivity, and superior fatigue resistance within one unit. The hydrogel, consisting of a PVA matrix with PEDOT:PSS as a conductive filler, features a topographical alignment that promotes axonal growth and achieves a fatigue threshold over  $500 \text{ J/m}^2$ , making it well-suited for sciatic nerve repairing. Phase segregation of PEDOT chains enhances its electrical conductivity ( $>500 \text{ S/m}$ ) and mitigates the interfacial impedance mismatch, allowing for high-efficiency bioelectrical signal transmission. *In vivo* studies on a rat sciatic nerve injury model corroborate the accelerated peripheral nerve regeneration through improved motor function recovery and efficient electrophysiological signal transmission. These findings establish our hydrogel-based NGCs as a promising solution for high-efficiency nerve regeneration through the synergy of topographical, mechanical, and electrical engineering.

**KEYWORDS:** conductive hydrogels, fatigue resistance, topographical geometry, nerve guidance conduits, nerve regeneration



## INTRODUCTION

The peripheral nervous system (PNS) possesses a complex and highly specialized structure that plays a critical role in its ability to transmit signals and regenerate after injury.<sup>1–5</sup> Peripheral nerve injuries (PNIs) are common and frequently occurring, often caused by surgical procedures, physical activities, or accidents.<sup>5–7</sup> PNIs may lead to the loss of sensory, motor, and cognitive functions, muscle paralysis, or even lifelong disability.<sup>4,6</sup> The gold-standard treatment for PNIs involves direct suturing for small gap defects (typically less than 5 mm) and autografts for larger gap defects exceeding 10 mm.<sup>5,8</sup> However, both suturing and autografts face several inherent challenges, including limited availability of donor nerves, surgical invasiveness, and morbidity at the donor sites, such as scarring, neuroma formation, or even loss of donor nerve functions. Moreover, unlike static tissues, peripheral nerves are frequently subjected to stretching, bending, and compression, particularly in regions around the joints and limbs.<sup>9–13</sup> Mechanical adaptability is critical for maintaining the structural and functional integrity of nerves in dynamic environments, which could not be achieved through direct suturing or autografts.<sup>2,10,11,14–16</sup> There is a pressing and long-standing

need for alternative strategies and materials for improved efficacy in nerve repair and regeneration.

Nerve guidance conduits (NGCs) made of biodegradable materials support nerve regeneration and functional recovery by providing structural support and a biomimetic environment.<sup>5,11,17–19</sup> These NGCs are typically fabricated from poly(L-lactide-*co*-*ε*-caprolactone) (PLLA-*ε*-CL), poly(lactic acid) (PLA), polycaprolactone (PCL), polyglycolic acid (PGA), or other biodegradable polymers, serving as scaffolds to provide structural support, guide axonal growth, and create a favorable microenvironment for nerve regeneration.<sup>19–21</sup> Despite these advancements, the efficacy of nerve regeneration using polymeric NGCs remains suboptimal due to several limitations. (1) Mechanical mismatch between polymeric NGCs (Young's modulus  $>100 \text{ MPa}$ ) and native nerve tissues

Received: January 14, 2025

Revised: April 13, 2025

Accepted: April 14, 2025

(50–500 kPa) causes nerve compression, leading to inflammation, neuroma formation, and impaired nerve regeneration.<sup>2,11,14</sup> (2) Poor permeability hinders nutrient diffusion and waste exchange, thus disrupting the local environment and delaying repairing.<sup>19,22</sup> (3) Lack of directional guidance results in misaligned axonal growth, reducing connectivity and delaying functional recovery.<sup>21,23</sup> (4) The absence of electrical conductivity limits bioelectrical signaling transduction, which is essential for Schwann cell activity, axonal alignment, and functional restoration.<sup>23–26</sup> These challenges highlight the need for synthetic NGCs with improved mechanical, structural, and electrical properties, alongside enhanced durability.

Hydrogel-based NGCs have emerged as promising tools for peripheral nerve repair due to their capability to replicate the natural extracellular matrix, supporting cell survival and efficient nutrient-waste exchange.<sup>27–29</sup> Conductive hydrogels, in particular, mimic the electrophysiological environment essential for bioelectrical signaling, promoting Schwann cell function, axonal regeneration, and myelination.<sup>3,24–26,30–33</sup> These materials also withstand the dynamic mechanical stresses encountered during daily body movements, such as stretching and compression, making them suitable for nerve repairing.<sup>2,34,35</sup> However, conventional hydrogels often fail under repeated mechanical loading, leading to fatigue-induced damage, crack propagation, and loss of structural integrity.<sup>9,15,36–38</sup> Such mechanical failure not only weakens the conduit but also disrupts uniform nerve regeneration, resulting in incomplete recovery or loss of functionality.<sup>9,11,32</sup> Addressing these challenges requires hydrogel-based NGCs with enhanced fatigue resistance, in order to maintain their structural and functional properties over prolonged application.<sup>36,37,39</sup> By achieving this, such materials could ensure consistent and reliable nerve repair, even in dynamic environments.

Herein, we report a kind of conductive hydrogel engineered with topographical alignment and mechanical robustness for improved PNI repair. The hydrogel mimics the topographical structure of nerve tissue, offering mechanical compliance and fatigue resistance while ensuring superior electrical conductivity through a continuous conductive polymer network. These features collectively support efficient bioelectrical signal transmission, which is essential for nerve regeneration. In a rat sciatic nerve injury model, the hydrogel-based NGCs synergistically enhance axonal growth, Schwann cell activity, and functional recovery through integrated electrical conductivity and precise surface topography. By integrating these crucial conductive, mechanical, and structural credentials within one system, our hydrogel NGCs offer a promising approach to improve nerve regeneration and address the limitations of traditional nerve repairing materials.

## RESULTS AND DISCUSSION

### Conductive Hydrogels with Topographical Features.

**Figure 1** and **Figure S1** schematically illustrate the design and fabrication of conductive hydrogel-based NGCs with tailored topographical features for nerve regeneration. The preferentially aligned microstructure and electron-ion hybrid conductivity, mimicking the nature of nerve tissues, synergistically offer an ideal pathway for nerve cell proliferation, directional alignment of nerve cell growth, and also bioelectrical signal conduction, thus accelerating nerve regeneration (**Figure 1a**). We selected poly(vinyl alcohol) (PVA) as the hydrogel

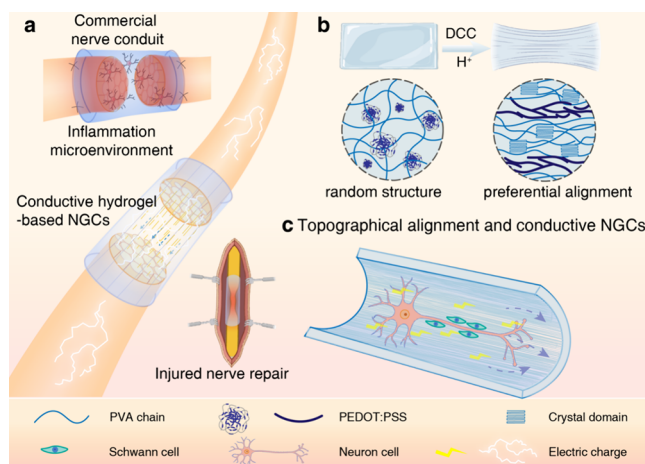


**Figure 1.** Schematic illustration of functional hydrogel-based NGCs for nerve regeneration. (a) Commercial nerve conduits (i.e., PCL or PGA) is challenged by mechanical mismatch, poor permeability, lack of directional guidance, and absence of electrical conductivity, thus leading to suboptimal efficacy of nerve regeneration. Conductive hydrogel engineered with topographical alignment and mechanical robustness could substantially improve PNIs repairing. (b) The hydrogel-based NGCs are composed of PVA and PEDOT:PSS. The topologically aligned structure is achieved through mechanical stretching, while subsequent solvent treatment induces the phase segregation of PEDOT chains and increase in conductivity. (c) The topologically aligned structure promotes the directional arrangement of nerve cell growth, while the conductive scaffold promotes neuroplasticity and enhances electrical signaling, thus facilitating function recovery.

backbone, in light of its superior aqueous solubility, biocompatibility, and tunable crystallinity. The topographical alignment was achieved through the classical drying-stretching technique,<sup>39</sup> by drying a freeze-thawed PVA hydrogel under mechanical stretching (**Figure 1b**). PEDOT:PSS, known for its intrinsically high conductivity and biocompatibility, was incorporated as the conductive filler.<sup>26</sup> However, in light of the presence of colloidal micelles of PEDOT:PSS within the PVA matrix, the as-obtained hydrogel materials exhibited an extremely low conductivity of 0.3 S/m, which is insufficient to offer an electrically conductive path. To solve this challenge, we further treated the hydrogel with volatile acid, i.e., acetic acid (HOAc), to induce the phase segregation of PEDOT chains, resulting in a sharp increase in conductivity. Additionally, we optimized the PEDOT:PSS filling ratio and systematically investigated the effect of different PEDOT:PSS concentrations (0.3, 0.6, 1.2, and 1.8 wt %) on the hydrogel's conductivity (**Figure S2**). Through comprehensive evaluation of electrical performance, material stability, and economic feasibility, 1.2 wt % was selected as the optimal filling ratio, resulting in a sharp increase in conductivity to 500 S/m.

The structural topography evolution of the hydrogel materials was investigated using scanning electron microscopy (SEM), revealing a transformation from a loose and random porous structure in the freeze-thawed PVA hydrogel (referred to as the random hydrogel, and abbreviated as A(−)E(−) hydrogel), to a preferentially aligned microstructure after drying-stretching treatment (referred to as the alignment hydrogel, and abbreviated as A(+)<sup>E(−)</sup> hydrogel), and ultimately to a preferentially aligned yet denser structure (referred to as the Aligned and Electron-conductive hydrogel, and abbreviated as AE hydrogel) (**Figure 2a,b**). The structural

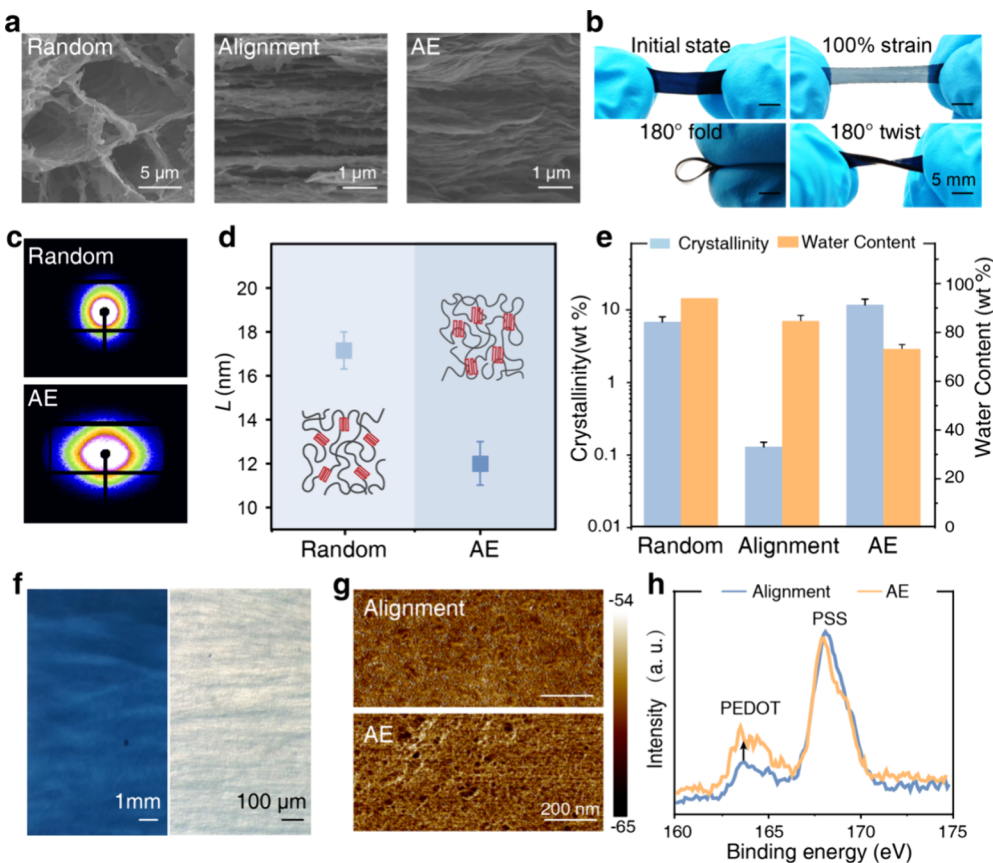


**Figure 2.** AE hydrogels with topologically aligned structures. (a) SEM images of hydrogel samples at each fabrication stage, the A(+)E(−), A(+)E(−), and AE hydrogel, disclosing the microstructural evolution during the fabrication process. The hydrogels evolved from a random porous structure to a preferentially aligned structure and finally the topologically aligned yet dense structure. (b) Images demonstrating the flexibility of our hydrogels, with the capability to readily twist, fold, and stretch up to a strain of 100% without damage. (c) Representative 2D SAXS patterns of the hydrogel samples corroborate the changes in structural alignment and crystallinity. (d) Summary of the averaged crystalline domain size ( $L$ ) for each hydrogel sample, as quantified from the SAXS measurement. (e) Comparison of the crystallinity and water content for each hydrogel sample. (f) Optical images showing the smooth and uniform surface for the hydrogels upon treatment with HOAc. (g) AFM images evidenced the fine nanostructure for the hydrogels treated with HOAc. (h) Representative XPS spectra revealed a shift in the binding energy of sulfur 2p electrons in PEDOT:PSS, corroborating the solvent-induced phase separation and formation of a conductive network upon treatment with HOAc.

alignment was also corroborated by confocal laser scanning microscopy (CLSM, Figure S3) observation and small-angle X-ray scattering measurement (SAXS, Figure 2c, and Figure S4). Additionally, SAXS analysis revealed a significant reduction in the interdomain distance from 17 to 12 nm among nanocrystalline domains ( $L$ ), underscoring the pivotal role of acid treatment in augmenting the polymer chain assembly and elevating the overall crystallinity (Figure 2d,e and Figure S5).

The continuity of the PEDOT conductive network was confirmed through additional characterization methods. As shown in Figure 2f, upon acid treatment, no precipitates were observed in the hydrogel matrix, but the topographical alignment was clearly visualized through microscopic imaging. Further atomic force microscopy (AFM) phase imaging (Figure 2g) disclosed the phase separation between PEDOT-rich (bright regions) and PSS-rich (dark regions) domains. This interconnected morphology promotes electron conductivity without sacrificing structural integrity.<sup>26</sup> On the other hand, change in binding energies of sulfur 2p electrons in PEDOT from XPS analysis (Figure 2h), together with the redshift in Raman spectra (Figure S6), corroborated the increased PEDOT-to-PSS ratio, as well as a structural transition of PEDOT from a benzoid to a quinoid

configuration, resulting in formation of continuous PEDOT network and increased conductivity (from 0.3 to 500 S/m).<sup>30,31</sup>

**Mechanical and Electrical Compliance of the AE Hydrogels.** The AE hydrogels, engineered with nerve-tissue-like structures, exhibited a topographically aligned architecture with improved mechanics, including high strength, stretchability, and flexibility. Similar to most biological tissues with anisotropic structures and mechanics, our hydrogel materials also exhibited anisotropy in mechanics, with a strength of 2 MPa and fracture strain of 200% along the alignment direction (//), which are much higher than that perpendicular to the alignment direction (⊥) (Figure 3a,b). The Young's modulus was quantified as 1000 kPa, comparable to that of biological tissues, i.e., sciatic nerves (~500 kPa), thus offering a mechanically compliant biointerface once it is used as artificial NGCs.

In the context of nerve regeneration, the ability to withstand large deformations and resist dynamical mechanical loading during the regeneration process is critical, as nerve tissues are more susceptible to deformation-related stresses than other biological tissues.<sup>9,26</sup> Similar to our previous findings, hydrogel materials with anisotropic structures and mechanics were also

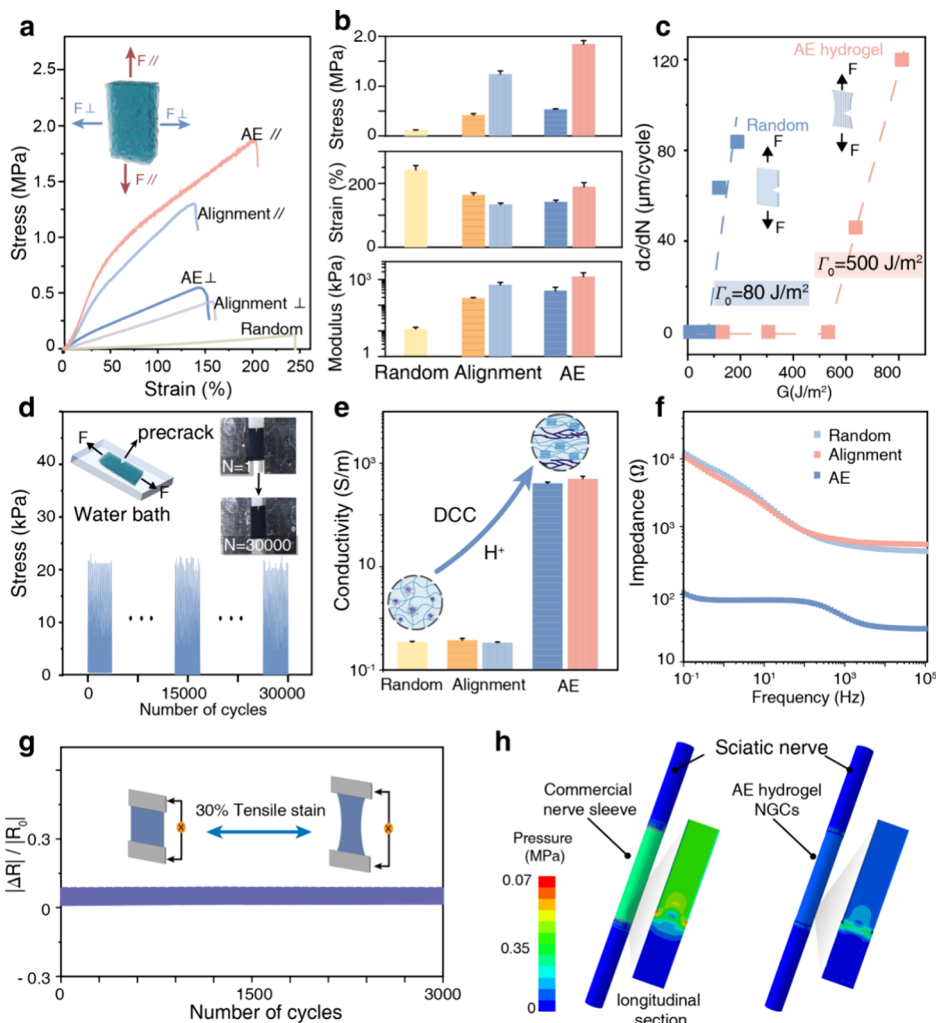


**Figure 3. Mechanical and electrical compliance of the AE hydrogels.** (a) Tensile stress–strain curves for hydrogel samples along parallel (//) and perpendicular (⊥) directions, featuring mechanical anisotropy. (b) Summary of strength, strain, and modulus for hydrogel samples in both directions. (c) AE hydrogels exhibit significantly higher fatigue thresholds ( $\Gamma_0 = 500 \text{ J/m}^2$ ) than the A(-)E(-) hydrogels ( $\Gamma_0 = 80 \text{ J/m}^2$ ). (d) Fatigue threshold validation of the AE hydrogels ( $N = 1, 15,000$ , and  $30,000$ ), showed no crack propagation during a  $30,000$  cycle fatigue test at an applied energy release rate of  $500 \text{ J/m}^2$ . (e) Electrical conductivity of hydrogel samples along two directions. (f) Impedance spectra of hydrogel samples demonstrate superior compatibility with biological tissues. (g) Relative resistance change ( $|\Delta R|/R_0$ ) of the AE hydrogel sample during cyclic tensile testing under  $30\%$  strain over  $3000$  cycles. (h) FEA comparing the stress distribution for the AE hydrogels and commercial nerve sleeves in contact with the sciatic nerve during nerve growth and expansion in the repairing process. Data in (b–c) and (e–f) are presented as means  $\pm$  S.D.,  $n = 3$ .

imparted with unprecedented resistance to fatigue crack propagation.<sup>36,37</sup> Using the single-notch technique, we were able to directly quantify the fatigue threshold, defined as the minimum fracture energy needed for fatigue crack propagation under cyclic deformation, as high as  $500 \text{ J/m}^2$ , significantly higher than that of the freeze–thawed random (A(-)E(-) hydrogel) samples ( $80 \text{ J/m}^2$ ). Furthermore, we have also validated the fatigue threshold by subjecting a prenotched AE hydrogel sample to an energy release rate of  $500 \text{ J/m}^2$  in the direction perpendicular to its alignment, and no noticeable crack propagation was observed upon  $30,000$  cycles of mechanical loading (Figure 3c,d; Figures S7 and Movie S1, Supporting Information). Collectively, these findings underscore our AE hydrogel's unique mechanical attributes, including superior strength, flexibility, and unprecedented fatigue resistance, essential for artificial NGCs for accelerated nerve regeneration.

In addition to their mechanical robustness, the AE hydrogels also exhibited impressive electrical properties, which are essential for nerve regeneration through improved bioelectrical signal transmission, promoting Schwann cell activity and nerve function recovery. Figure 3e showed that the conductivity of AE hydrogels reached approximately  $500 \text{ S/m}$ , greatly exceeding that of A(-)E(-) hydrogels without acid treatment (with conductivities of  $\sim 0.3 \text{ S/m}$ ). This high conductivity could be ascribed to the well-formed yet continuous PEDOT conductive pathway within the hydrogel matrix, thus enabling efficient electron transportation. The plotting of resistance change ( $|\Delta R|/R_0$ ) against strain is closely aligned with the ideal elastomeric conductor model, with a slight variation in resistance with the increase in strain (Figure S8). Additionally, the AE hydrogels demonstrated exceptionally low impedance across a wide frequency range ( $40 \Omega$ , Figure 3f), nearly 3 orders of magnitude lower than that of nerve tissues ( $5–50 \text{ k}\Omega$ ).<sup>25</sup> The combination of low impedance, long-term stability

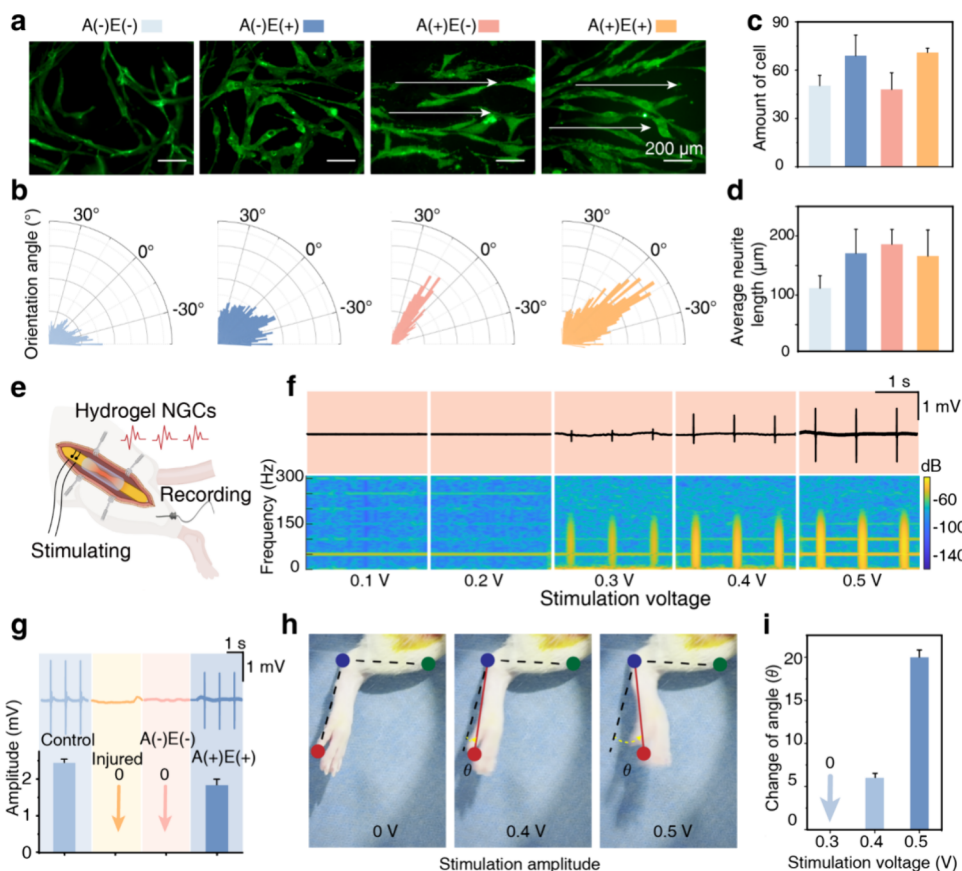


**Figure 4.** AE hydrogel as NGCs for structural guidance and electrophysiological intervention against the biological systems. (a) Fluorescence images showing the morphology of neurons cultured on different hydrogel samples. The arrows indicate aligned neurite growth. (b) Polar plots illustrate the orientation angle distribution of neurites in each group ( $n = 3$ ). (c, d) Quantitative analysis on cell amount and average neurite length in each hydrogel group ( $n = 3$ ). (e) Schematic illustration of the hydrogel NGCs for electrical stimulation and recording against the nerve systems. (f) Representative electrophysiological signals were recorded through our AE hydrogel, upon activation at different stimulation voltages and corresponding 2D spectrograms. (g) Representative electrophysiological signals were recorded from an injured sciatic nerve through various hydrogel samples. The injured nerve and nerve wrapped with  $A(-)E(-)$  hydrogel are not conductive, while the AE hydrogels can provide a reliable conductive pathway. (h, i) Images showing movement of the ankle joints in response to different stimulation voltages (h), and a summary of movement angles (i), corroborating the voltage-dependent nerve activation. Data in panels (c, d, f, g, and i) are presented as means  $\pm$  S.D.,  $n = 3$ .

of electron conductivity, and excellent mechanical stability in simulated biological fluids (Figures S9 and S10) ensures efficient signal transmission while minimizing interfacial resistance, making AE hydrogels highly advantageous for electronic biointerfacing.<sup>33</sup> Furthermore, the dynamic electrical stability of the AE hydrogels was further confirmed through cyclic stretching tests. As shown in Figure 3g, relative resistance change was measured under 30% tensile strain (the maximum stretch ratio that the nerve can achieve) over 3000 cycles. Even after prolonged deformation,  $|\Delta R|/R_0$  remained within a minimal fluctuation range of 0 to 0.1. This demonstrates the AE hydrogel's outstanding electrical stability and fatigue resistance, making it well-suited for repeated mechanical deformation during nerve repair. In addition to providing a stable electrophysiological environment, superior mechanical compliance is essential for nerve guidance conduits to avoid excessive pressure on the nerves during the repairing process. The long-term soaking of our AE hydrogels in PBS buffer over 48 h did not result in significant volumetric expansion. Specifically, the length remained unchanged, while the swelling ratio in width was less than 200%, and below 250% for thickness. Consequently, the hydrogels would not

impose mechanical compression on the nerves when used as artificial NGCs (Figure S11).

Finite element analysis (FEA) was conducted to simulate the interaction between AE hydrogel-based NGCs and nerve tissues during the repairing process, with commercially available nerve conduits (Neurolac, PCL-based,  $\sim 50$  MPa) tested for comparison. During nerve growth and expansion, commercial conduits exhibited uneven stress distribution, with maximal stress reaching up to 0.35 MPa, which could potentially compress the nerves. In contrast, AE hydrogels displayed uniform stress distribution, with maximal stress below 0.07 MPa, ensuring superior mechanical compliance and reducing the risk of nerve damage (Movie S2, Supporting Information). These findings validate the ability of AE hydrogels to maintain stable conductivity under dynamic mechanical stress while providing a mechanically compliant biointerface. To further understand the mechanical behavior of the hydrogel-nerve system and its interfacial mechanical compatibility, we developed a mechanical model based on volumetric growth theory (Figure S12). The results indicated that the radial Cauchy stress induced by the AE hydrogel was

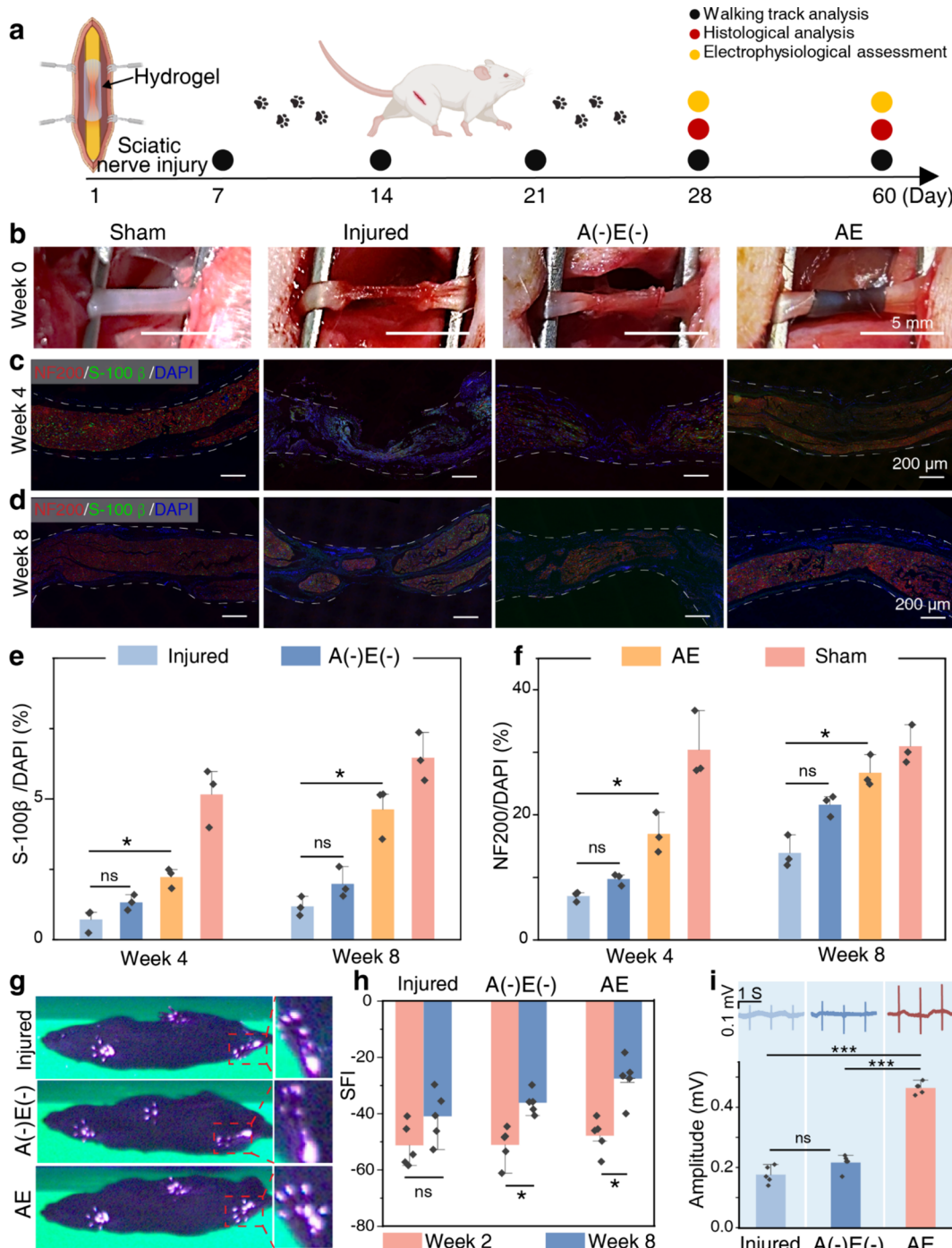


**Figure 5. AE Hydrogels as NGCs for the accelerated repairing of injured sciatic nerves.** (a) Schematic illustration of the experimental timeline for repairing the injured sciatic nerve using our AE hydrogel-based NGCs, with key assessment time points for walking track analysis, histological analysis, and electrophysiological assessment during the 60-day repairing. (b) Images of the injured sciatic nerves repairing with different hydrogel NGCs at week 0. Scale bar: 5 mm. (c, d) Immunofluorescent staining of NF200 (red) and S-100 $\beta$  (green) markers in the repaired nerve tissues at weeks 0 and 8, with DAPI (blue) staining for cell nuclei. (e, f) Quantification of S-100 $\beta$ -positive cells (e) and NF200-positive cells (f) over DAPI in different treatment groups. (g) Representative images of walking track analysis showing the footprint patterns in different treatment groups. (h) Summary of sciatic functional index (SFI) at weeks 0 and 8 for the repaired sciatic nerves in different hydrogel groups. (i) Representative electrophysiological patterns through the repaired sciatic nerves and summary of maximal signal amplitude for different hydrogel groups. Data in panels (e) and (f) are presented as means  $\pm$  S.D.,  $n = 3$ , while data in panels (h) and (i) are presented as means  $\pm$  S.D.,  $n = 5$ .

significantly lower than that caused by the commercial nerve conduits.

**AE Hydrogels for Electrophysiological Signal Transmission.** To investigate the biocompatibility of our AE

hydrogels as artificial NGCs, PC12 cells were seeded on the hydrogel substrates. The AE hydrogel matrices exhibited superior cytocompatibility during a 7-day cell culture with the nerve cells, as corroborated by both qualitative and

quantitative cell viability tests (Figure S13). To probe the effects of topological geometry on nerve cellular behaviors, PC12 cells were cultured on the AE hydrogel substrates and induced with nerve growth factor (NGF) for differentiation. For comparison, other hydrogel substrates were also tested, including pure PVA hydrogel with neither alignment nor electron-conductivity (denoted as A(−)E(−)), PVA/PE-DOT:PSS hydrogel (denoted as A(−)E(+)), and topologically aligned PVA hydrogel (denoted as A(+)E(−)). In light of the synergy from electron conductivity and alignment in the topological surfaces, cells on our AE hydrogels preferentially aligned along the nanostructured alignment cues (indicated by arrows), indicating the role of topological alignment for promoting directional neuron growth (Figure 4a). In sharp contrast, randomly distributed PC12 cells were observed for those hydrogel substrates without topological alignment, such as the A(−)E(−) and A(−)E(+) groups. From the statistical analysis, with a comparable amount of cells for each group, most cells accumulated and aligned around 0° in the AE and A(+)E(−) hydrogel groups, indicating strong directional growth guided by the substrate's topological cues (Figure 4b–d).

To further validate the capability of our AE hydrogels for *in vivo* electrophysiological signal transmission, we first performed the frog muscle contraction experiment to confirm their capability to deliver immediate electrical triggers at the nerve-tissue interface (Figure S14). Building upon these results, we proceeded to the rat sciatic nerve electrical stimulation tests, where we evaluated the AE hydrogel's performance in a more physiologically relevant model for nerve repair. We then built an injured sciatic nerve in a rat model by surgically transecting the sciatic nerve and creating a gap of 5 mm, following previously reported protocols (Movie S3, Supporting Information).<sup>18</sup> The injured sciatic nerve was then wrapped with our AE hydrogels, while A(−)E(−) hydrogels of the same dimension were tested as a control (Figure 4e, Movie S4, Supporting Information). We then conducted electrical stimulation at one end and recorded the electrophysiological signal at the other end. With a stimulation voltage below 0.2 V, no electrophysiological signal could be monitored, indicating insufficient stimulation to elicit a measurable nerve signal (Figure 4f,g and Figure S15). The signal could be recorded at a threshold voltage of 0.3 V; after that, a gradual increase in stimulation voltage was accompanied by increased signal amplitude. Electrical signals were effectively transmitted from the stimulated nerve through the AE hydrogels, across the gap, to the other end of the nerve to conduct the electrical signals.

To isolate the effects of AE hydrogel-mediated electrophysiological signal transmission from external electrical stimulation, we did not administer continuous electrical stimulation to promote nerve regeneration during the study. Instead, electrical stimulation was only applied to evaluate the intrinsic conductive properties of AE hydrogels in bridging the injured nerve gap. In this case, the subsequent nerve regeneration could be solely ascribed to the hydrogel's ability to restore electrophysiological signal transmission, rather than from exogenous electrical stimulation. We also tested gold electrodes of the same size for comparison, and a threshold voltage of 0.9 V was quantified following the same protocol (Figure S16), due to the intrinsic mismatch in electrical impedance between the metallic electrodes and biological tissues.<sup>16,32</sup> Additionally, our hydrogel materials can function as an interface for delivering electrical stimulation, effectively

triggering macroscopic body movements. For instance, upon being subjected to electrical stimulation (0.4–0.5 V, 1 Hz frequency, biphasic charge-balanced rectangular pulses), consistent and periodic movement of the ankle joints (~20°) was observed (Figure 4h,i and Movie S5, Supporting Information). It demonstrated reliable stimulation of the sciatic nerves, showing potential for restoring or modulating motor functions. The nerve-tissue interface constructed through the AE hydrogels enabled immediate tissue-to-tissue biointerfacing, thus enabling further nerve tissue repair with the assistance of AE hydrogel-based NCGs.

**AE Hydrogels for Accelerated Sciatic Nerve Regeneration.** Given the superior performance of our AE hydrogels in integrating topographical geometry with conductive properties to promote nerve alignment and electrical signal transmission, we then validated their potential in repairing nerve defects as artificial NCGs for the functional recovery of injured nerves. In our animal experiment, the AE hydrogel group was conducted as the experimental group, while the Sham-operated group, the Injured group, and the A(−)E(−) group served as controls. Additionally, the Sham group provides a baseline reference, as these animals underwent the surgical procedure without nerve injury. Due to our rigorous and well-established surgical modeling techniques, the Sham group only experienced superficial skin incisions without muscle or nerve damage (Movie S3, Supporting Information). Figure 5a illustrates the experimental timeline, detailing the walking track analysis, histological evaluation, and electrophysiological tests over a 60 day period, ensuring a holistic assessment of nerve repair. Figure 5b presents macroscopic images of the sciatic nerves following the successful establishment of the injury model and subsequent treatment with AE hydrogel-based NCGs, with A(−)E(−) hydrogels used as a control. Histological analysis, including HE staining, revealed that the AE hydrogel group achieved nearly complete nerve reconnection after 8 weeks of repairing, demonstrating significantly improved outcomes compared to the Sham group and the A(−)E(−) hydrogel group (Figures S17 and S18).

Immunofluorescence staining for NF200 and S-100 $\beta$  at 4 and 8 weeks postinjury (Figure 5c,d) highlights the superior regeneration capacity of AE hydrogels.<sup>23</sup> S-100 $\beta$ , a Schwann cell marker reflecting early repair processes, showed significantly higher expression in the AE hydrogel group at week 4 (2.5%) compared with the A(−)E(−) hydrogel group (1.2%). This elevated S-100 $\beta$  level indicates active Schwann cell proliferation, creating a supportive environment for axonal growth. By week 8, S-100 $\beta$  levels in the AE hydrogel group stabilized at 5%, matching those observed in normal nerves, while those in the A(−)E(−) group remained at 3%, reflecting delayed repairing progress. Similarly, NF200 expression, a marker for axonal maturation, remained low in the AE hydrogel group at week 4 (20%) but increased significantly to 25% by 8 weeks, indicating rapid axonal elongation and maturation (Figure 5f and Figure S20). In contrast, the A(−)E(−) group only reached 18% at week 8, a level comparable to that of the AE hydrogel group at week 4, underscoring the accelerated regeneration facilitated by AE hydrogels. The combined analysis of S-100 $\beta$  and NF200 demonstrates that AE hydrogels expedite both Schwann cell activity in the early phase and axonal maturation in the late phase of nerve repair. These results, coupled with minimal inflammation and well-organized nerve tissues observed at

week 8 (Figures S18 and S21), further validate the efficacy of AE hydrogels in enhancing nerve regeneration and functional recovery.

We subsequently performed walking track analysis to evaluate the sciatic function index (SFI) following NGC implantation, which serves as a critical parameter for assessing motor function recovery. Following our previously reported protocol,<sup>29</sup> walking track analysis was utilized to further investigate motor function restoration. In this evaluation, an SFI of  $-100$  indicates a complete loss of motor function, while an SFI of  $0$  represents full functional recovery.<sup>32</sup> At week 2, all experimental groups exhibited severe deficits, with SFI values ranging from  $-50$  to  $-60$ , indicating a slight recovery. At week 8, the injured group remained impaired without any treatment, with an SFI around  $-40$ , comparable to that of the A(–)E(–) hydrogel group ( $SFI \approx -35$ ), while our AE hydrogel group could achieve a near-normal level with an SFI of  $-30$ . Since the Sham group recovered completely within 1 day ( $SFI = 0$ ), it was not included in longitudinal functional assessments such as SFI and CMAP measurements, as it did not exhibit functional deficits postsurgery. The electrophysiological data of the Sham group are referenced in Figure 4g for comparison. These results aligned with the histological data (Figure 5c,d and Figure S22), suggesting that the AE hydrogel's conductive properties enabled electrophysiological signal transmission and facilitated motor recovery. Figure 5i displays compound muscle action potential (CMAP) curves, assessing the nerve electrical conduction capability of the static nerves after 8 weeks of repair. Both the injured group and the A(–)E(–) hydrogel group demonstrated moderate improvement, with CMAP amplitudes of  $\sim 0.2$  mV, while  $0.4$  mV was detected for the AE hydrogel group, approaching the value of the normal groups. This remarkable improvement corroborates that the conductive properties of AE hydrogels enhance the hydrogel's ability to facilitate efficient signal transmission, promoting functional integration of regenerating axons with target muscles (Figure S23).

## CONCLUSIONS

In summary, we developed a kind of conductive hydrogel-based NGCs that overcome the limitations of traditional nerve repairing materials by integrating topographical structures, enhanced electroactivity, and superior fatigue resistance within a single platform. Compared with conventional hydrogels, our AE hydrogel exhibits remarkable fatigue resistance with a fatigue threshold of  $500$  J/m<sup>2</sup>, meeting the durability requirements necessary for peripheral nerve repairing. Furthermore, the AE hydrogel's high electrical conductivity ( $500$  S/m) and low impedance enable efficient neural signal transmission at the nerve-hydrogel interface, thus facilitating nerve regeneration. In vivo experiments using a rat sciatic nerve injury model demonstrated that the AE hydrogel-based NGC significantly promoted nerve regeneration, improved motor function, and effectively transmitted electrophysiological signals.

Future studies should focus on optimizing the degradation profile, refining the electrical conductivity parameters, and investigating the long-term integration of the hydrogel NGC within complex neural environments. Moreover, large-animal models and multiomics analyses will be essential to systematically map the hydrogel NGC's influence on neural regeneration at the molecular level. Before clinical translation, further validation is required to define implantation strategies,

safety profiles, and patient-specific customization. Although in its early stages, the AE hydrogel-based NGC represents an innovative approach for nerve repair, offering new perspectives and directions for the development of next-generation neural repairing strategies. By bridging biomaterials, neural engineering, and functional bioimplants, this platform has the potential to advance both fundamental neuroscience and clinical neurotherapeutics.

## MATERIALS AND METHODS

**Finite Element Analysis for Stress Concentration (FEA).** A three-dimensional model of a nerve cuff interacting with nerve tissue was constructed in an Abaqus CAE to perform finite element analysis (FEA). The model presupposed ideal bonding at all contact interfaces, with both the cuff and the nerve tissue represented as homogeneous, isotropic, and hyperelastic materials. The nerve tissue was represented as a hollow cylinder with a diameter of  $1$  mm and a length of  $15$  mm, including a  $5$  mm damaged segment at its center. Similarly, the test material was constructed as a hollow cylindrical structure featuring an inner diameter of  $1$  mm, an outer diameter of  $1.5$  mm, and a height of  $6$  mm, enveloping the outer surface of the nerve tissue. External loads were applied to the outer layer of the test material to analyze the stress distribution transmitted to the underlying nerve tissue.

**In Vivo Sciatic Nerve Stimulation.** All samples underwent preparation and were sterilized by exposure to ultraviolet (UV) light for  $3$  h. Male SD rats (weighing  $200$ – $300$  g, supplied by Charles River Co., Ltd.) were anesthetized with isoflurane (1–3%) delivered in oxygen. After the fur on the thigh region was shaved, a skin incision was made to reveal the subcutaneous tissue. The sciatic nerve was exposed through careful dissection of the lateral femoris and biceps femoris muscles. AE hydrogel, A(–)E(–) hydrogel, and a gold electrode were applied directly to the injured sciatic nerve. Sham-operated and injured-only groups were used as controls. Neural stimulation was performed using a biphasic, charge-balanced rectangular voltage pulse (1 Hz, 0.1–1 V). Commercial electrodes (Taimeng Chengdu, BL420N) were used to record electrical activity from the nerve and associated muscle, while a protractor placed beneath the legs was used to measure the ankle joint angle. The recorded signals were sampled at  $1$  kHz and processed using MATLAB 2023b software.

**Surgical Procedure.** All animal procedures were conducted in strict accordance with the guidelines approved by the Ethics Committee of the Southern University of Science and Technology (SUSTech) (protocol number: SUSTech-JY202304002). The surgical protocols were reviewed and approved by the Committee on Animal Care at SUSTech. Male Sprague–Dawley (SD) rats (weighing  $200$ – $300$  g, provided by Charles River Co., Ltd.) were used as experimental subjects in this study.

The rats were randomly divided into four experimental groups ( $n = 24$  per group): the Sham group, the injury group, the A(–)E(–) hydrogel group, and the AE hydrogel group. A sciatic nerve crush injury model was established as described in previous studies.<sup>29,32</sup> During the procedure, the rats were anesthetized with 1–2 vol.% isoflurane delivered in oxygen, ensuring continuous anesthesia throughout the surgery. The sciatic nerve of the left hind limb was exposed, and a  $5$  mm segment was crushed using surgical forceps (Oscar, China) under a microscope for  $1$  min. In the Sham group, the sciatic nerve was exposed but not subjected to injury, and the incision was immediately sutured postoperatively. The Injury group consisted of rats that received no material-based treatment after nerve injury. For the A(–)E(–) hydrogel group, the injured nerve was wrapped with A(–)E(–) hydrogel (namely, PVA hydrogel,  $\sim 5$  mm in length and  $\sim 3$  mm in width), serving as a nerve conduit. Similarly, in the AE hydrogel group, the injured nerve was enclosed with the AE hydrogel as a conduit. To enhance the stability and prevent displacement, a tiny amount of bioadhesive was applied around the hydrogel to ensure firm attachment to the nerve tissue. This fixation method eliminates the need for suturing, minimizing additional tissue trauma and

inflammation. To comply with animal welfare guidelines, post-operative pain management was implemented immediately following surgery. Meloxicam was administered subcutaneously at a dose of 2 mg kg<sup>-1</sup> once daily for 7 days to reduce pain and improve animal comfort.

**Footprint Analysis.** At 2, 4, and 8 weeks following implantation, gait analysis was conducted according to established methodologies. The rats were trained to traverse a specialized runway equipped with a footprint recording system. During each session, the footprints of the rats were captured, and the sciatic functional index (SFI) was calculated for each group using the following formula:

$$\text{SFI} = \frac{108.44(E_{PL} - N_{PL})}{N_{PL}} + \frac{13.3(E_{TS} - N_{TS})}{N_{TS}} + \frac{31.85(E_{ITS} - N_{ITS})}{N_{ITS}}$$

In this equation, PL represents paw length, TS corresponds to toe spread (the distance between the first and fifth toes), and ITS indicates intermediary toe spread (the distance between the second and fourth toes). The symbol *E* denotes the experimental group subjected to surgical intervention, while the symbol *N* refers to the normal control group without surgery.

## ASSOCIATED CONTENT

### Supporting Information

The Supporting Information is available free of charge at <https://pubs.acs.org/doi/10.1021/acsnano.5c00845>.

Materials and methods; synthetic procedures; instrumentation and measurements including SEM, CLSM, DSC, TGA, SAXS, and mechanical tests; animal tests for sciatic nerve regeneration; histological and immunohistochemical analysis; SAXS, DSC, and Raman spectra of the hydrogels; stability of electrical conductivity; swelling behaviors; cytotoxicity; electrophysiological signals under various stimulation voltages; hematological analysis; histological evaluation of sciatic nerve repairing; immunofluorescence staining of sciatic nerve sections; gait analysis and of muscle recovery (PDF)  
Fatigue resistance of AE hydrogels (MP4)  
FEA of the hydrogel-tissue interface (MP4)  
Sciatic nerve positioning (MP4)  
Construction of sciatic nerve injury model (MP4)  
Electrical stimulation over sciatic nerve (MP4)

## AUTHOR INFORMATION

### Corresponding Author

Ji Liu – Department of Mechanical and Energy Engineering, Southern University of Science and Technology, Shenzhen 518055, China;  [orcid.org/0000-0001-7171-405X](https://orcid.org/0000-0001-7171-405X); Email: [liuj9@sustech.edu.cn](mailto:liuj9@sustech.edu.cn)

### Authors

Yinghui Feng – Department of Mechanical and Energy Engineering, Southern University of Science and Technology, Shenzhen 518055, China

Liangjie Shan – Department of Mechanical and Energy Engineering, Southern University of Science and Technology, Shenzhen 518055, China

Yafei Wang – Department of Mechanical and Energy Engineering, Southern University of Science and Technology, Shenzhen 518055, China

Xingmei Chen – Department of Mechanical and Energy Engineering, Southern University of Science and Technology, Shenzhen 518055, China

Chang Wang – Department of Mechanical and Energy Engineering, Southern University of Science and Technology, Shenzhen 518055, China

Complete contact information is available at:  
<https://pubs.acs.org/10.1021/acsnano.5c00845>

### Author Contributions

<sup>2</sup>Y.F. and L.S. contributed equally to this work.

### Author Contributions

The manuscript was written through contributions from all authors. All authors have given approval to the final version of the manuscript.

### Notes

The authors declare no competing financial interest.

## ACKNOWLEDGMENTS

The authors acknowledge the financial support by STI 2030-Major Projects (2022ZD0209500), the National Natural Science Foundation of China (52373139 and U2436202), the Guangdong Basic and Applied Basic Research Foundation (2024A1515240042), the Basic Research Program of Shenzhen (JCYJ20230807093419041, 20231116101626002, and JCYJ20240813094159001), and China Postdoctoral Science Foundation (2024M751289). The authors also gratefully acknowledge the support from the Shenzhen Science and Technology Innovation Commission (KJZD20240903101400001) and the Development and Reform Commission of Shenzhen Municipality (XMHT20240115003). The authors would also like to acknowledge the technical support from SUSTech Core Research Facilities.

## REFERENCES

- (1) Lacour, S. P.; Courtine, G.; Guck, J. Materials and technologies for soft implantable neuroprostheses. *Nat. Rev. Mater.* **2016**, *1* (10), 16063.
- (2) Choi, Y. S.; Hsueh, Y. Y.; Koo, J.; Yang, Q.; Avila, R.; Hu, B.; Xie, Z.; Lee, G.; Ning, Z.; Liu, C.; Xu, Y.; Lee, Y. J.; Zhao, W.; Fang, J.; Deng, Y.; Lee, S. M.; Vázquez-Guardado, A.; Stepien, I.; Yan, Y.; Song, J. W.; Haney, C.; Oh, Y. S.; Liu, W.; Yoon, H. J.; Banks, A.; MacEwan, M. R.; Ameer, G. A.; Ray, W. Z.; Huang, Y.; Xie, T.; Franz, C. K.; Li, S.; Rogers, J. A. Stretchable, dynamic covalent polymers for soft, long-lived bioresorbable electronic stimulators designed to facilitate neuromuscular regeneration. *Nat. Commun.* **2020**, *11* (1), 5990.
- (3) Jin, S.; Choi, H.; Seong, D.; You, C. L.; Kang, J. S.; Rho, S.; Lee, W. B.; Son, D.; Shin, M. Injectible tissue prosthesis for instantaneous closed-loop rehabilitation. *Nature* **2023**, *623* (7985), 58–65.
- (4) Wang, L.; Lu, C.; Yang, S.; Sun, P.; Wang, Y.; Guan, Y.; Liu, S.; Cheng, D.; Meng, H.; Wang, Q.; He, J.; Hou, H.; Li, H.; Lu, W.; Zhao, Y.; Wang, J.; Zhu, Y.; Li, Y.; Luo, D.; Li, T.; Chen, H.; Wang, S.; Sheng, X.; Xiong, W.; Wang, X.; Peng, J.; Yin, L. A fully biodegradable and self-electrified device for neuroregenerative medicine. *Sci. Adv.* **2020**, *6* (50), No. eabc6686.
- (5) Zhou, W.; Rahman, M. S. U.; Sun, C.; Li, S.; Zhang, N.; Chen, H.; Han, C. C.; Xu, S.; Liu, Y. Perspectives on the Novel Multifunctional Nerve Guidance Conduits: From Specific Regenerative Procedures to Motor Function Rebuilding. *Adv. Mater.* **2024**, *36* (14), No. e2307805.
- (6) Shen, J.; Sun, Y.; Liu, X.; Chai, Y.; Wang, C.; Xu, J. Nerve Regeneration Potential of Antioxidant-Modified Black Phosphorus Quantum Dots in Peripheral Nerve Injury. *ACS Nano* **2024**, *18* (34), 23518–23536.
- (7) Kang, X.; Li, X.; Liu, C.; Cai, M.; Guan, P.; Luo, Y.; Guan, Y.; Tian, Y.; Ren, K.; Ning, C.; Fan, L.; Tan, G.; Zhou, L. A shape-

- persistent plasticine-like conductive hydrogel with self-healing properties for peripheral nerve regeneration. *J. Mater. Sci. Technol.* **2023**, *142*, 134–143.
- (8) Singh, V. K.; Haq, A.; Tiwari, M.; Saxena, A. K. Approach to management of nerve gaps in peripheral nerve injuries. *Injury* **2022**, *53* (4), 1308–1318.
- (9) Liu, X.; Rao, S.; Chen, W.; Felix, K.; Ni, J.; Sahasrabudhe, A.; Lin, S.; Wang, Q.; Liu, Y.; He, Z.; Xu, J.; Huang, S.; Hong, E.; Yau, T.; Anikeeva, P.; Zhao, X. Fatigue-resistant hydrogel optical fibers enable peripheral nerve optogenetics during locomotion. *Nat. Methods* **2023**, *20* (11), 1802–1809.
- (10) Zheng, Z.; Chen, X.; Wang, Y.; Wen, P.; Duan, Q.; Zhang, P.; Shan, L.; Ni, Z.; Feng, Y.; Xue, Y.; Li, X.; Zhang, L.; Liu, J. Self-Growing Hydrogel Bioadhesives for Chronic Wound Management. *Adv. Mater.* **2024**, *36* (41), No. 2408538.
- (11) Cao, S.; Wei, Y.; Bo, R.; Yun, X.; Xu, S.; Guan, Y.; Zhao, J.; Lan, Y.; Zhang, B.; Xiong, Y.; et al. Inversely engineered biomimetic flexible network scaffolds for soft tissue regeneration. *Sci. Adv.* **2023**, *9* (39), No. eadi8606.
- (12) Lin, S.; Liu, J.; Liu, X.; Zhao, X. Muscle-like fatigue-resistant hydrogels by mechanical training. *Proc. Natl. Acad. Sci. U. S. A.* **2019**, *116* (21), 10244–10249.
- (13) Freedman, B. R.; Kuttler, A.; Beckmann, N.; Nam, S.; Kent, D.; Schuleit, M.; Ramazani, F.; Accart, N.; Rock, A.; Li, J.; Kurz, M.; Fisch, A.; Ullrich, T.; Hast, M. W.; Tinguley, Y.; Weber, E.; Mooney, D. J. Enhanced tendon healing by a tough hydrogel with an adhesive side and high drug-loading capacity. *Nat. Biomed. Eng.* **2022**, *6* (10), 1167–1179.
- (14) Chen, X.; Feng, Y.; Zhang, P.; Ni, Z.; Xue, Y.; Liu, J. Hydrogel Fibers-Based Biointerfacing. *Adv. Mater.* **2024**, *37*, No. 2413476.
- (15) Seo, H.; Han, S. I.; Song, K. I.; Seong, D.; Lee, K.; Kim, S. H.; Park, T.; Koo, J. H.; Shin, M.; Baac, H. W.; et al. Durable and Fatigue-Resistant Soft Peripheral Neuroprosthetics for In Vivo Bidirectional Signaling. *Adv. Mater.* **2021**, *33* (20), No. e2007346.
- (16) Xue, Y.; Chen, X.; Wang, F.; Lin, J.; Liu, J. Mechanically-Compliant Bioelectronic Interfaces through Fatigue-Resistant Conducting Polymer Hydrogel Coating. *Adv. Mater.* **2023**, *35* (40), No. 2304095.
- (17) Liu, A. P.; Appel, E. A.; Ashby, P. D.; Baker, B. M.; Franco, E.; Gu, L.; Haynes, K.; Joshi, N. S.; Kloxin, A. M.; Kouwer, P. H. J.; et al. The living interface between synthetic biology and biomaterial design. *Nat. Mater.* **2022**, *21* (4), 390–397.
- (18) Xuan, H.; Wu, S.; Jin, Y.; Wei, S.; Xiong, F.; Xue, Y.; Li, B.; Yang, Y.; Yuan, H. A Bioinspired Self-Healing Conductive Hydrogel Promoting Peripheral Nerve Regeneration. *Adv. Sci.* **2023**, *10* (28), No. 2302519.
- (19) Vijayaventaraman, S. Nerve guide conduits for peripheral nerve injury repair: A review on design, materials and fabrication methods. *Acta Biomater.* **2020**, *106*, 54–69.
- (20) Namhongsa, M.; Daranarong, D.; Sriyai, M.; Molloy, R.; Ross, S.; Ross, G. M.; Tuantranont, A.; Tocharus, J.; Sivasinprasas, S.; Topham, P. D.; et al. Surface-modified polypyrrole-coated PLCL and PLGA nerve guide conduits fabricated by 3D printing and electrospinning. *Biomacromolecules* **2022**, *23* (11), 4532–4546.
- (21) Wang, J.; Xiong, H.; Zhu, T.; Liu, Y.; Pan, H.; Fan, C.; Zhao, X.; Lu, W. W. Bioinspired Multichannel Nerve Guidance Conduit Based on Shape Memory Nanofibers for Potential Application in Peripheral Nerve Repair. *ACS Nano* **2020**, *14* (10), 12579–12595.
- (22) Lord, M.; Whitelock, J.; Turnbull, J. E. Better growth-factor binding aids tissue repair. *Nat. Biomed. Eng.* **2020**, *4* (4), 368–369.
- (23) Xu, D.; Fu, S.; Zhang, H.; Lu, W.; Xie, J.; Li, J.; Wang, H.; Zhao, Y.; Chai, R. Ultrasound-Responsive Aligned Piezoelectric Nanofibers Derived Hydrogel Conduits for Peripheral Nerve Regeneration. *Adv. Mater.* **2024**, *36* (28), No. e2307896.
- (24) Park, J.; Jeon, J.; Kim, B.; Lee, M. S.; Park, S.; Lim, J.; Yi, J.; Lee, H.; Yang, H. S.; Lee, J. Y. Electrically Conductive Hydrogel Nerve Guidance Conduits for Peripheral Nerve Regeneration. *Adv. Funct. Mater.* **2020**, *30* (39), No. 2003759.
- (25) Bedard, C.; Piette, C.; Venance, L.; Destexhe, A. Extracellular and intracellular components of the impedance of neural tissue. *Biophys. J.* **2022**, *121* (6), 869–885.
- (26) Li, G.; Huang, K.; Deng, J.; Guo, M.; Cai, M.; Zhang, Y.; Guo, C. F. Highly Conducting and Stretchable Double-Network Hydrogel for Soft Bioelectronics. *Adv. Mater.* **2022**, *34* (15), No. e2200261.
- (27) Chen, Z.; Zhang, H.; Fan, C.; Zhuang, Y.; Yang, W.; Chen, Y.; Shen, H.; Xiao, Z.; Zhao, Y.; Li, X.; Dai, J. Adhesive, stretchable, and spatiotemporal delivery fibrous hydrogels harness endogenous neural stem/progenitor cells for spinal cord injury repair. *ACS Nano* **2021**, *16* (2), 1986–1998.
- (28) Han, S.; Gao, L.; Dou, X.; Wang, Z.; Yang, K.; Li, D.; Yuan, Y.; Xing, C.; Jiang, B.; Tian, Y.; Feng, C. L.; Zhang, P. Chiral hydrogel nerve conduit boosts peripheral nerve regeneration via regulation of Schwann cell reprogramming. *ACS Nano* **2024**, *18* (41), 28358–28370.
- (29) Zhang, J.; Chen, X.; Lin, J.; Zhang, P.; Lei, I. M.; Tao, Y.; Zhang, J.; Luo, T.; Liu, J. Hydrogel bioadhesives harnessing nanoscale phase separation for Achilles tendon repairing. *Nano Research* **2024**, *17* (2), 778–787.
- (30) Zhou, T.; Yuk, H.; Hu, F.; Wu, J.; Tian, F.; Roh, H.; Shen, Z.; Gu, G.; Xu, J.; Lu, B.; Zhao, X. 3D printable high-performance conducting polymer hydrogel for all-hydrogel bioelectronic interfaces. *Nat. Mater.* **2023**, *22* (7), 895–902.
- (31) Chong, J.; Sung, C.; Nam, K. S.; Kang, T.; Kim, H.; Lee, H.; Park, H.; Park, S.; Kang, J. Highly conductive tissue-like hydrogel interface through template-directed assembly. *Nat. Commun.* **2023**, *14* (1), 2206.
- (32) Zhang, J.; Wang, L.; Xue, Y.; Lei, I. M.; Chen, X.; Zhang, P.; Cai, C.; Liang, X.; Lu, Y.; Liu, J. Engineering electrodes with robust conducting hydrogel coating for neural recording and modulation. *Adv. Mater.* **2023**, *35* (3), No. 2209324.
- (33) Zhang, P.; Yang, Y.; Li, Z.; Xue, Y.; Wang, F.; Shan, L.; Wang, Y.; Shi, X.; Wu, K.; Liu, J. Conducting Hydrogel-Based Neural Biointerfacing Technologies. *Adv. Funct. Mater.* **2025**, No. 2422869.
- (34) Jiang, C.; Zhang, L.; Yang, Q.; Huang, S.; Shi, H.; Long, Q.; Qian, B.; Liu, Z.; Guan, Q.; Liu, M.; Yang, R.; Zhao, Q.; You, Z.; Ye, X. Self-healing polyurethane-elastomer with mechanical tunability for multiple biomedical applications in vivo. *Nat. Commun.* **2021**, *12* (1), 4395.
- (35) Zhang, M.; An, H.; Gu, Z.; Huang, Z.; Zhang, F.; Jiang, B. G.; Wen, Y.; Zhang, P. Mimosa-Inspired Stimuli-Responsive Curling Bioadhesive Tape Promotes Peripheral Nerve Regeneration. *Adv. Mater.* **2023**, *35* (32), No. 2212015.
- (36) Liang, X.; Chen, G.; Lin, S.; Zhang, J.; Wang, L.; Zhang, P.; Lan, Y.; Liu, J. Bioinspired 2D Isotropically Fatigue-Resistant Hydrogels. *Adv. Mater.* **2022**, *34* (8), No. 2107106.
- (37) Liang, X.; Chen, G.; Lin, S.; Zhang, J.; Wang, L.; Zhang, P.; Wang, Z.; Wang, Z.; Lan, Y.; Ge, Q.; Liu, J. Anisotropically fatigue-resistant hydrogels. *Adv. Mater.* **2021**, *33* (30), No. 2102011.
- (38) Huang, S.; Liu, X.; Lin, S.; Glynn, C.; Felix, K.; Sahasrabudhe, A.; Maley, C.; Xu, J.; Chen, W.; Hong, E.; Crosby, A. J.; Wang, Q.; Rao, S. Control of polymers' amorphous-crystalline transition enables miniaturization and multifunctional integration for hydrogel bioelectronics. *Nat. Commun.* **2024**, *15* (1), 3525.
- (39) Li, X.; Gong, J. P. Design principles for strong and tough hydrogels. *Nat. Rev. Mater.* **2024**, *9* (6), 380–398.